Dynamics of Dust Aggregates in a Complex Plasma

Allen B. Davis, Jorge A. Carmona-Reyes, Lorin S. Matthews, and Truell W. Hyde
Center for Astrophysics, Space Physics and Engineering Research, Baylor University,
Waco, Texas 76798-7310, USA

***Abstract*—Dust aggregates in complex plasmas have been studied theoretically in computer models, but not extensively in an experimental setting. This work investigates several properties of aggregates which are responsible for dust dynamics: charge, dipole moment, and gas drag. A diode pumped laser is used to perturb aggregates in a GEC rf reference cell, and a high-speed camera acquires image data. Particle trajectories are extracted and analyzed to characterize or estimate values of the properties under investigation.**

***Index Terms*—Aggregates, Dipole moment, Dust charge, Dusty plasma, Gas drag.**

I. Introduction

Dusty plasmas can be found in such diverse celestial environments as comet tails, planetary rings, and interstellar clouds [1]. Small, micrometer-sized dust particles in plasma can collide under certain conditions to form aggregate structures. Charged dust aggregates play an important role in many astrophysical phenomena, such as early stages of protostellar and protoplanetary growth, the dynamics of planetary rings and cometary tails, and the formation of noctilucent clouds in earth's upper atmosphere [2]. Dust is also expected to be an unwanted byproduct in the operation of plasma fusion devices, such as ITER [3]. In all of these environments, direct study of the dust aggregates in their *in situ* environment is extremely difficult, if not impossible.

As a model for these complex plasma environments, dust aggregates are formed in a laboratory plasma as monodisperse spheres are accelerated in a self-excited dust density wave. Individual dust particles are perturbed using a diode pumped solid state laser (coherent VERDI) with their motions recorded by a high-speed camera. Analysis of the particle motion allows determination of the aggregate characteristics, such as charge, mass, and gas drag. Although these quantities have been studied in computer models [2], little experimental data has been acquired and analyzed to date.

Manuscript received August 2012. This work was supported in part by the National Science Foundation under Grant No. 0847127 through the Research Experience of Undergraduates program. This work was also supported by the Baylor Department of Physics.

Allen B. Davis is an undergraduate at Williams College, Williamstown, MA 01267 USA, and was a participant in the REU program (e-mail: allen.b.davis@williams.edu).

Jorge Carmona-Reyes is with the Center for Astrophysics, Space Physics & Engineering Research, Baylor University, Waco, TX. 76798 USA (e-mail: Jorge_Carmona@baylor.edu).

Lorin S. Matthews is with the Physics department at Baylor University, Waco, TX 76798 (email: Lorin_Matthews@baylor.edu).

Truell W. Hyde is with the Center for Astrophysics, Space Physics & Engineering Research, Baylor University, Waco, TX. 76798 USA (phone: 254-710-3763, fax: 254-710-7309, e-mail: Truell_Hyde@baylor.edu).

II. Theory

A. Charging

A dust aggregate acquires an electric charge by colliding with the constituent electrons and ions in the plasma. Electrons in the plasma have a significantly greater velocity than the ions due to their lower mass. Thus an aggregate experiences a greater flux of electrons than ions, giving the aggregate a negative charge. The aggregate's negative charge will eventually repel incoming electrons at the same rate that it attracts ions, leading to an equilibrium charge. An aggregate's electric charge affects its interactions with other nearby aggregates in the plasma as well. Since aggregates tend to all be charged negatively, they resist collisional growth. However, high velocities can allow aggregates to overcome their electrostatic repulsion and collide and stick [4].

B. Levitation

In this experiment, a GEC rf (Gaseous Electronics Conference radio frequency) reference cell is used to study dust aggregate interactions in plasma under laboratory conditions. A description of this setup and relevant terminology can be found in [5]. Dust introduced to the

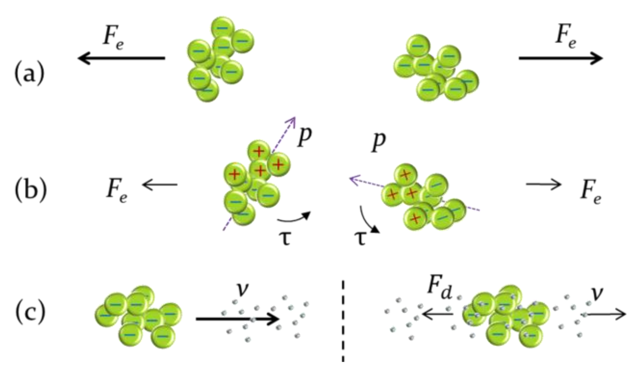

Fig. 1. This drawing depicts the three aggregate interactions studied in this work: (a) is the electrostatic repulsion of two negatively charged aggregates, (b) is the dipole interaction of two aggregates with a charge distribution, and (c) is the deceleration of an aggregate due to gas drag.

plasma acquires a charge as described above. Single dust particles (monomers) or aggregate structures can levitate in the plasma with a negative charge, as a result of the balancing gravitational and electromagnetic forces, given by

$$mg = qE \tag{1}$$

where m is the mass of the dust aggregate, g is gravitational acceleration, q is the total charge on the aggregate, and E is the downward electric field in the plasma sheath.

C. Electrostatic Force

Nearby aggregates can interact at a distance through electrostatic forces, given by

$$F_e = \frac{k_e q_1 q_2}{r^2} \tag{2}$$

where k_e is the Coulomb constant, q_1 and q_2 are the charges of the two aggregates, and r is the distance between the aggregates. These forces are attractive if the particles are oppositely charged or repulsive if they are similarly charged. See Fig. 1 (a) for an illustration. In a GEC rf reference cell, it can be assumed that all suspended particles have a negative net charge, since positive net charges would not be able to counter the gravitational force and remain aloft.

D. Dipole Interactions

A typical dust aggregate is not charged uniformly across its surface. As monomers collide and stick, the resulting aggregate rapidly acquires some equilibrium charge distribution, depending on the arrangement of the monomers within the aggregate. Aggregates can have complex structures, and similarly complex charge distributions, giving them a dipole moment. An external electric field applies a torque to such an aggregate, causing it to spin. This torque is given by

$$\tau = p \times E \tag{3}$$

where τ is the torque, p is the dipole moment, and E is the uniform, external electric field. The dipole moment points from negative charge towards positive charge by convention. In this experiment, the plasma sheath provides the electric field, but nearby charged aggregates contribute their own electric fields as well. This means that aggregates can affect their neighbors' spins. See Fig. 1 (b) for an illustration. Dipole effects can also allow aggregates with a negative net charge to attract one another in spite of their electrostatic repulsion [6].

E. Gas Drag

The motion of the dust in the plasma is limited by gas drag. Moving dust collides with the electrons, ions, and neutral atoms in the plasma. For weakly ionized plasmas, we consider only neutral gas drag because it dominates the ion drag [7]. This drag force is be given by

$$F_d = \beta v \tag{4}$$

where F_d is the drag force, β is the gas drag coefficient, and v is the velocity of the particle. β is an experimentally determined value. See Fig. 1 (c) for an illustration.

When perturbed, dust particles can oscillate about some equilibrium position. The decay rate of the oscillation is related to β. An oscillator can be measured using the equation

$$2\pi \frac{U_s}{U_d} = Q = \frac{\sqrt{mk}}{\beta} \tag{5}$$

where U_s is the energy stored in the oscillator, U_d is the energy dissipated each cycle, Q is the quality factor, m is the particle mass, k is the effective spring constant, and β is the same gas drag coefficient from (4).

III. Experimental Setup

This paper addresses two experiments: Expt. 1 and Expt. 2. Both experiments were conducted in a GEC rf reference cell located in the Center for Astrophysics, Space Physics & Engineering Research (CASPER) lab at Baylor University [8]. See Fig. 2 for a schematic. A glass cube, 1 inch on each side, sits on the lower electrode and provides horizontal confinement to the dust aggregates. The cube has an open top face to allow the dust to enter when dropped from above. Argon plasma is ignited with the lower electrode set to oscillate its voltage at 13.56 MHz.

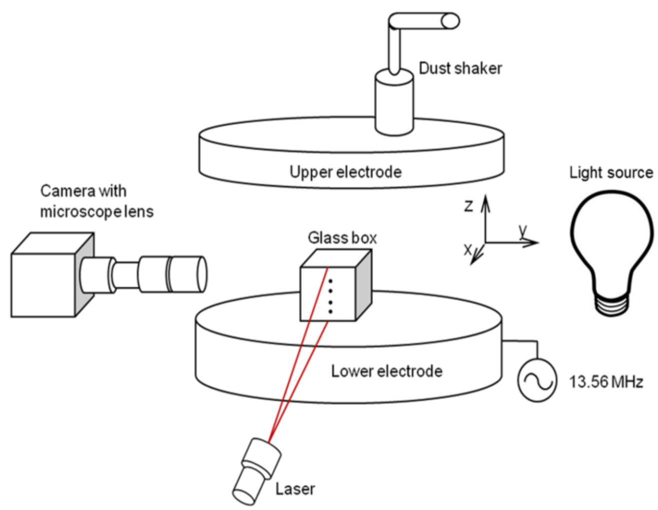

Fig. 2. This is a schematic of the setup of both experiments. Aggregates are confined within the glass box inside the GEC rf reference cell. The camera images the aggregate's silhouettes against the light source behind the glass box, outside of the cell. The laser was used only in Expt. 2 to perturb aggregates.

A dust shaker is manually concussed several times to sprinkle monomer dust grains into the plasma. The spherical grains are made of melamine formaldehyde with gold coating and have a diameter of 8.94 μm and mass of 0.61 ng.

A high-speed Photron 1024PC CMOS camera equipped with a microscopic lens is placed outside a window of the chamber, pointing horizontally between the electrodes towards a face of the glass box. On the other side of the chamber, a floodlight shines towards the camera through the glass box. This light allows the camera to see the dust aggregates as dark silhouettes against a bright background. Silhouettes not in the focal plane of the camera appear large and blurry.

The aggregates are formed from the monomers by lowering the gas pressure for ten seconds. This creates a dust density wave, allowing for higher relative velocities between the grains [9]. Colliding monomers stick at the point of contact to form aggregates, containing from two to thirty monomers. The pressure is then restored to allow the dust to return to their lower relative velocities. Interactions between these drifting aggregates within the camera's field of view are analyzed.

A 532-nm diode pumped solid state laser (coherent VERDI) is aligned to enter a third window perpendicular to the camera's line of sight. The laser beam is spread into a vertical sheet which is used to perturb aggregates in the camera's field of view.

A. *Experiment 1*

Large aggregates are created in the cell (approximately 10-30 monomers comprising each) after several dust density waves. The plasma pressure is set to 500 mTorr. Data is gathered at 3000 fps. The laser is not used in this experiment.

B. *Experiment 2*

Smaller, more compact aggregates are created in the cell (approximately 4-10 monomers comprising each). The plasma pressure is set to 466 mTorr. Data is gathered at 2000 fps. The laser is manually switched on and off several times per second during data acquisition. Aggregates passing through the laser are pushed and appear bright with scattered laser light.

IV. DATA PROCESSING

Tens of thousands of images are acquired in both experiments. Each image sets is examined and moments of interest to the project are selected. Special care is made to pick out interactions which take place within the focal plane of the camera. Although it is difficult to precisely determine the distance of an aggregate from the focal plane, it is evident to the eye when events occur along the same plane.

ImageJ is used first to format raw images for analysis. For Expt. 1 data, hundreds of image frames are loaded into the program. A pixel value threshold is set, which converts the greyscale image into a binary image of black or white; all pixel values greater than the threshold become white, while all those below the threshold become black.

Images acquired in Expt. 2 must be preprocessed in *MATLAB* and *ImageJ* (Fig. 3). Since the laser causes a dark aggregate to become whiter than the background, a single-point threshold would be unable to capture both the dark silhouettes and the bright glows of the aggregates. Using a *MATLAB* script command, a two-point threshold is set based upon deviations from the median pixel value in an image sequence. The script produces a new binary image from each original image, setting the lowest pixel values to black, while also setting the highest values to black. The middle range of pixel values is set to white.

This method can cause aggregates to appear fragmented, as in Fig. 3 (b). *ImageJ* can solve this problem through Dilate and Erode functions. The Dilate function expands the black (aggregate) pixels, whereas the Erode function expands the white (background) pixels. Several iterations of Dilate allow broken up aggregate images to become whole. Then the Erode function is applied an equal number of times to restore the particles to approximately their original size. Although this process can distort the shape of the aggregate slightly, its position is sufficiently accurate. Dilate and Erode were not used in Expt. 1, so the shapes in that data set are not degraded.

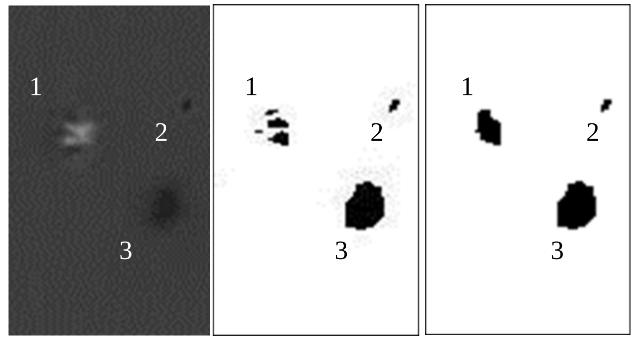

(a) (b) (c)

Fig. 3. An image from Expt. 2 is depicted at three stages of processing: (a) is raw image data, (b) is the image produced by *MATLAB*'s two-point threshold script, and (c) is the previous image after Dilate and Erode functions are used in *ImageJ*. In each of the above: (1) is an aggregate partially illuminated by the laser, (2) is a stationary flaw in the camera, and (3) is a typical aggregate silhouette.

V. PARTICLE TRACKING

Once images have been converted to binary images, *ImageJ*'s Analyze Particles function is used to obtain numerical values for particles' positions and orientations (Fig. 4). The user enters parameters for particle detection: pixel area and circularity. These values are adjusted as needed to ensure detection of the desired particle(s). In some cases it is necessary to manually delete nearby flaws or ancillary particles to properly detect target particles.

Analyze Particles is set to fit ellipses snuggly around the particles it detects and to output the following data into a text file: x and y pixel positions, area of the ellipse, and angle of the ellipse's major axis to the horizontal. The function has no tracking capabilities, so the output file is merely a list of detected particles from the top pixel in the first frame to the bottom pixel in the last frame. For this reason, it is critical to know that the target particle is detected in each frame, and that if non-target particles are detected at all, they are detected in every frame. Otherwise it becomes impossible to automate the upcoming sorting process.

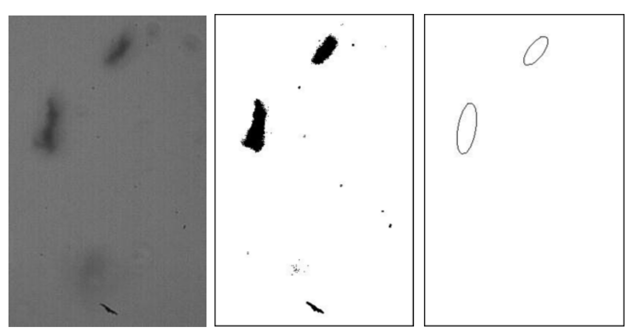
(a) (b) (c)

Fig. 4. (a) depicts an image from Expt. 1 in its raw form. (b) depicts the image after a threshold has been set. (c) depicts the ellipses fit around the aggregates. Notice that the faint particle near the bottom of (a) and the speckles in (b) have been filtered out in (c).

The text output is imported into *MATLAB*, where a script is run to extract alternating rows of data and assign it to variables representing each particle detected. If two particles pass one another in the y-pixel coordinate, the script automatically reverses the parity of the sorting from that point onwards to anticipate the reversal in output order, as described above.

Once the data are sorted, a polynomial function is fit to the x and y position data. The fits do not model a physical situation, but merely act as a smoothing spline. Velocity and acceleration are calculated from these fit curves.

By counting the pixel size of an in-focus monomer within an aggregate, it is possible to estimate conversion factor between pixels and physical distance. For both data sets, one pixel is approximately equal to 1.4 μm.

Graphs are produced for the position, velocity, acceleration, separation, and angle of the aggregates involved in the interaction. It is possible to compare aggregates whose data sets are temporally separated by setting a time offset. Most of the graphs shown here were produced in this manner.

VI. Results

A. Experiment 1

The large aggregates created in this experiment (approximately 10-30 monomers comprising each) are conducive to measurements of charge and dipole moment.

Fig. 5 shows the close interaction of two particles (P1 and P2). P1 enters the frame first on the lower right, rotating slowly about a vertical axis. P2 enters next from the top on a course to collide with P1. As they approach one another, their paths are deflected and they miss each other. P1's angle shifts drastically as it passes P2.

P1 is estimated to be comprised of ten monomers, and P2 is estimated to be comprised of 22 monomers. A closer view of P2 is available in Fig. 6.

Fig. 7 shows a graph of each particle's acceleration in the x-direction. The acceleration in the y-direction is trivial, so physical values can be taken from the x-direction alone.

Fig. 8 shows a graph of each particle's angle. This measurement is based on the angle that the major axis of an ellipse fit to each particle makes to the horizontal.

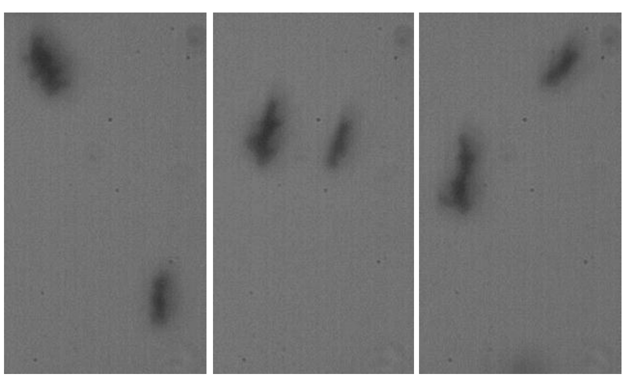

(a) (b) (c)

Fig. 5. These three frames from Expt. 1 show the first interaction being considered. (b) is the closest approach between the particles. P1 begins in the bottom right, P2 begins in the top left.

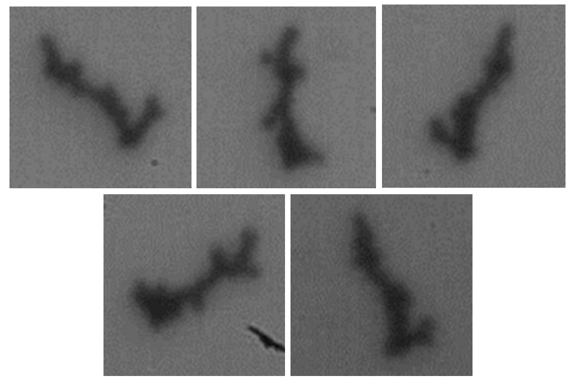

Fig. 6. Particle 2 is shown at five points throughout its rotation. The first and fifth images are approximately one completely rotation apart; the aggregate is experiencing nutation. These were the most in-focus images of Particle 2 that were acquired.

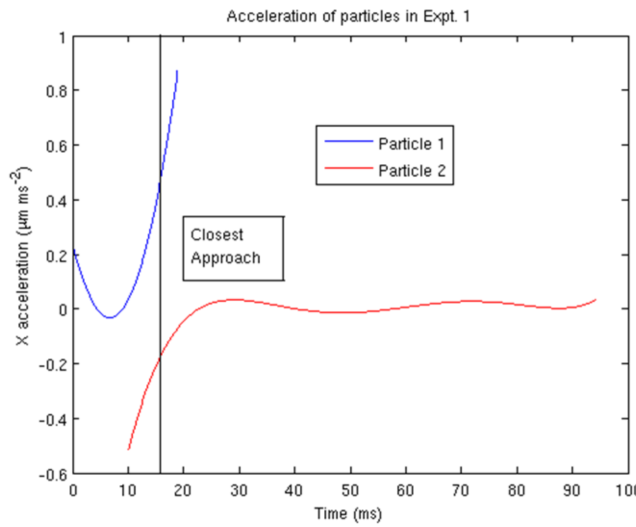

Fig. 7. This graph was derived from a polynomial fit of position vs. time data in Expt. 1. It shows the x-accelerations of P1 and P2 during their interaction. The vertical black line indicates the point when the two particles were closest to one another in x-accelerations.

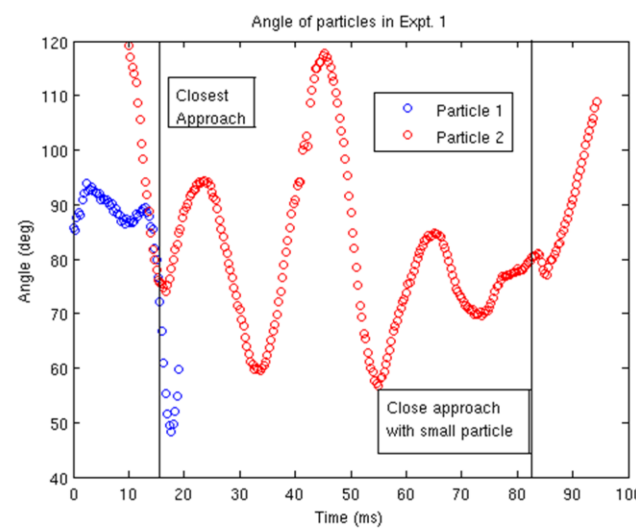

Fig. 8. This graph plots the angle that P1 and P2 make to the horizontal. The vertical black line on the left indicates where P1 and P2 are closest in the x-direction. The vertical black line on the right indicates a disturbance in P2's angle resulting from another encounter with a small, out-of-focus aggregate.

P2 was observed at another point in the dataset during an interaction with a small, compact particle (P3). This interaction is shown in Fig. 9. A graph of the angles of P2 and P3 is shown in Fig. 10.

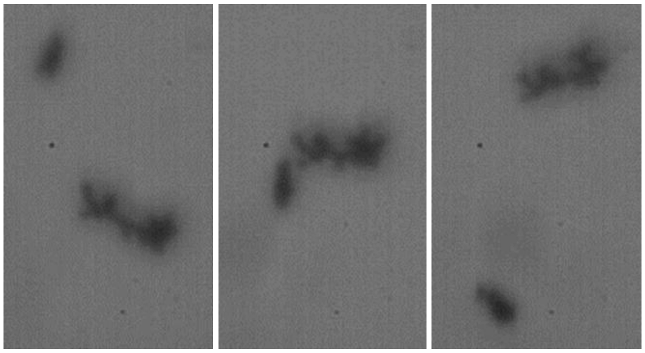

(a) (b) (c)

Fig. 9. Three frames are shown here from the second interaction considered in Expt. 1. (b) is the closest approach between the particles. P2 begins in the bottom right. P3 begins in the top left.

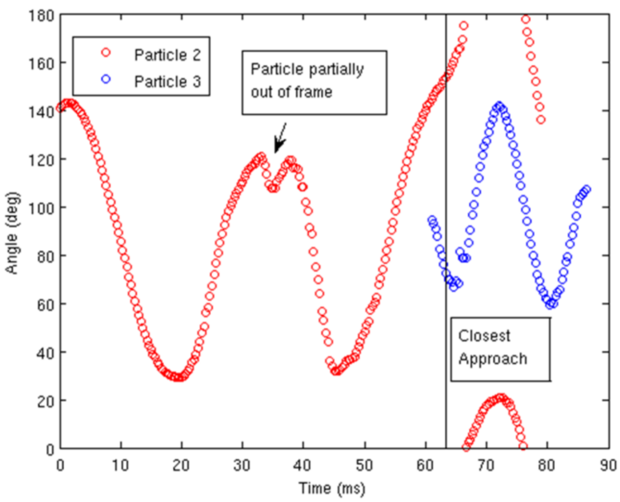

Fig. 10. This graph plots the angle that P2 and P3 make to the horizontal. The anomaly near t=35 results from P2 dropping partially out of the camera's field of view; the bottom is obscured, which affects its angle measurement due to its asymmetry. Shortly after the closest approach (indicated by the vertical black line), there is a discontinuity in the plot for P2 because it flips past the horizontal, causing the ellipse's other end to register as a low angle number instead.

B. Experiment 2

Smaller, more compact aggregates are created in the cell (approximately 4-10 monomers comprising each). The laser is switched on and off rapidly, providing brief impulses to aggregates within the laser's plane. This experiment was conducive to measuring gas drag.

Fig. 11 depicts a particle (comprised of about seven monomers) being perturbed by the laser sheet. It moves from right to left. Once the laser is turned off, it sloshes back towards its original position, following the same path. This motion is graphed in Fig. 12. The laser turns on again before the particle's motion has fully ceased, displacing it once more.

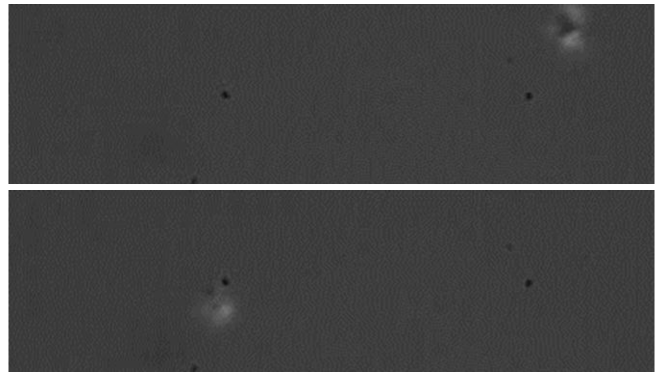

Fig. 11. In these raw images from Expt. 2, the laser 2 blasts the particle from right to left. A light glow surrounds the particle from the scattered laser light. The two dark spots in each image are flaws in the camera.

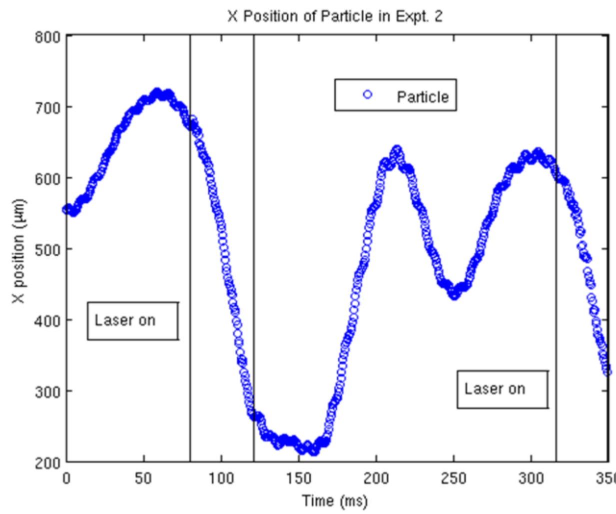

Fig. 12. This graph shows the position of the particle in Expt. 2 as it is perturbed by the laser. The two vertical black lines on the left indicate the duration of the first laser blast. The vertical black line on the left indicates the start of the next blast, which continues until after graph terminates. The low amplitude, high frequency (120 Hz) oscillations result from camera shaking, and do not adversely affect the data.

VII. Conclusion

A. Charge Estimation (Expt. 1)

Using (2), it is possible to estimate a charge on P1 and P2 with the data in Fig. 7. There is no way from the data alone to separate q_1 from q_2, but we can make a plausible estimation by assuming that the charge to mass ratio is the same for both aggregates. The value of $q_1 q_2$ is 2.89×10^{-30} C. P1 has ten monomers, and P2 has 22 monomers. So we will assume that q_2 = (22/10) q_1. Then a substitution gives q_1 = -1.1×10^{-15} C and q_2 = -2.5×10^{-15} C. We know the net charges are negative from (1), because only negative net charges will be able to overcome the gravitational force to float in the plasma sheath.

The ratio of the accelerations in Fig. 7 can give an idea of the accuracy of the mass ratio estimation (i.e. monomer count) because the electrostatic force should be symmetric. A simple division of the accelerations at the point of least separation yields 0.32. This does differ from the mass ratio estimate of 10/22 ≈ 0.45 by about 30%. This is a moderate discrepancy likely resulting from two assumptions which were made in the calculations: that the particles' pre- and post-interaction trajectories were on the same plane and that the accelerations measured were purely in the x-direction. Furthermore, there is uncertainty in the count of monomers in the two aggregates. The ratio of pixels to μm is also approximate, but this should not affect the mass ratio estimate. If the charges of q_1 and q_2 are recalculated using a mass ratio of 0.32 (based on acceleration data alone) and with the same q_1q_2 value as before, then $q_1 = -9.6\times10^{-16}$ C and $q_2 = -3.0\times10^{-15}$ C.

It is also possible that dipole effects are responsible for making the interaction asymmetrical. There could be an exchange of kinetic and rotational energy that makes pure acceleration data insufficient to account for all the energy in the system. Strong dipoles can also attract each other despite having similar net charges, which would complicate the problem [6].

B. *Dipole Estimation (Expt. 1)*

The interaction of P1 and P2 depicted in Fig. 5 shows the obvious rotation of P1 in response to P2's proximity. This rotation can also be clearly seen in the angle vs. time plot in Fig. 8. It is evident from Fig. 5 (c) that bottom end of P1 is attracted to the top end of P2. This would indicate that the dipole moments of the two aggregates are aligned in generally the same direction: either both up or down (pointed towards positive y or negative y in the images). Given the long, thin shape of the aggregates, it seems very plausible that the dipole moments would be along this axis.

By examining an interaction between P2 and a new particle, P3, it is possible to determine which of the two possible directions the dipole moments of P1 and P2 are pointing. In Fig. 9, P3 passes very close to P2. P3 is smaller and more compact than P1. These facts mean that its dipole moment must be comparatively small, because the charge lacks the room to separate very far. Since P3 is levitating, like all the aggregates in the data, it has a net negative charge. So we can treat P3 as a point negative charge, at least for the purpose of inferring P2's dipole moment. In Fig. 9 (c) the "top" of P2 bobs to follow P3 downwards (see Fig. 6 for P2's typical rotation and "top"). This motion is visible in Fig. 10 which shows a shift in P2's angle when it is closest to P3; it bobs so far that the usual "top" dips beneath the horizontal, causing a discontinuity in the angle plot. The fact that P2's "top" is attracted to the negatively charged P3 indicates that P2's "top" is positively charged. Since we have established that P1 and P2 have dipole moments in the same direction, we can conclude that the dipole moment of P1 and P2 both point upwards. This reasoning is illustrated in Fig. 13. Whether or not this upward orientation is the norm for aggregates in the plasma sheath is grounds for further investigation.

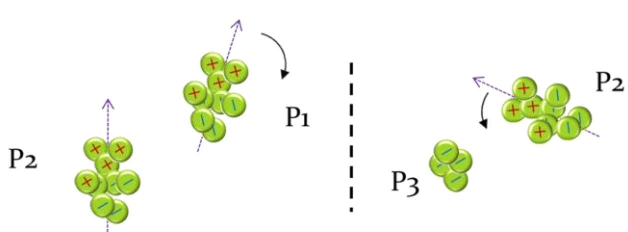

Fig. 13. This is an illustration of the suspected dipole moments of the three particles considered in Expt. 1. Notice that the torques are directed to bring opposite charged areas closer together. The motions depicted are directly from the data, but the charge distributions are extrapolated.

C. *Gas Drag Estimation (Expt. 2)*

Fig. 12 shows a particle as it is perturbed by a laser and begins oscillating back towards its equilibrium position. The particle overshoots the equilibrium point, and it turns around again near 200 ms. This means that the oscillator is underdamped. Using (5), we can estimate the Q of the system if we assume that the particle is a harmonic oscillator and that the potential well is parabolic. With these assumptions we get that $E \propto A^2$, where E is the energy of the wave and A is the wave's amplitude. Only about one and a half periods of oscillation are visible before the laser is switch on again, but it appears that the amplitude of the oscillation decreases by a factor of two. We can then extrapolate that ¾ of the remaining kinetic energy is dissipated during each oscillation. Equation (5) gives Q = 8.4. The mass of the aggregate is known by counting the monomers comprising the particle (thought to be seven). This leaves k and β as the only unknowns in (5). A determination of the effective spring constant should be a goal of future work, so that an informed estimate of β can be made.

Acknowledgment

Allen B. Davis thanks Dr. Jie Kong for his guidance in using *ImageJ* to identify and track particles. The author thanks Patrick Murray for his *MATLAB* advice and for stimulating conversations which led to some of this work's conclusions. The author also thanks Kathleen Higgins for discussing the basis for dipole orientation determination. And finally the author thanks Baylor University's CASPER program for this unique opportunity.

References

[1] V. E. Fortov, A. G. Khrapak, S. A. Khrapak, V. I. Molotkov, O. F. Petrov, "Dusty plasma," *Physics-Uspekhi*, vol. 47, no. 5, pp. 447-492, 2004.
[2] L. S. Matthews, R. L. Hayes, M. S. Freed, T. W. Hyde, "Formation of Cosmic Dust Bunnies," *IEEE Trans. Plasma. Sci.*, vol. 35, no. 2, pp. 260-265, 2007.
[3] V. Chuyanov, L. Topilski, "Prevention of hydrogen and dust explosion in ITER," *Fusion Engineering and Design*, vol. 81, pp. 1313-1319, 2006.
[4] L. S. Matthews, T. W. Hyde, "Effect of dipole-dipole charge interactions on dust coagulation," *New J. Physics*, vol. 11, 063030, 2009.
[5] V. Land, E. Shen, B. Smith, L. Matthews, T. Hyde, "Experimental and computational characterization of a modified GEC cell for dusty plasma experiments," *New J. Physics*, vol. 11, 063024, 2009.
[6] G. Lapenta, "Effect of Dipole Moments on the Coagulation of Dust Particles Immersed in Plasmas," *Physica Scripta*, vol. 57, pp. 476-480, 1998.
[7] S. Khrapak and G. Morfill, "Basic Processes in Complex (Dusty) Plasmas: Charging, Interactions, and Ion Drag Force", *Contrib. Plasma Phys.* vol. 49, no. 3, pp. 148-168, 2009.
[8] J. Kong, T. W. Hyde, L. Matthews, K. Qiao, Z. Zhang, and A. Douglass, "One-dimensional vertical dust strings in a glass box", *Phys. Rev. E*, vol. 84, 016411, 2011.
[9] C. Du, H. M. Thomas, A. V. Ivlev, U. Konopka, G. E. Morfil, "Agglomeration of microparticles in complex plasmas," *Phys. Plasmas*, vol. 17, 113710, 2010.

Allen B. Davis was born in New London, CT, in 1992. He is a graduate of Deerfield Academy and is currently an undergraduate astrophysics major at Williams College, Williamstown, MA. He participates in jazz band (trombone), the fencing team, and the Monday Night Hearts Club.
He is a member of the 2012 Center for Astrophysics, Space Physics, & Engineering Research summer program at Baylor University, Waco, TX.

Jorge Carmona-Reyes received the B.S. degree in physics from Southern Nazarene University, Bethany, OK, and the M.S. degree in physics from Baylor University, Waco, TX. He is currently with Baylor University, where he is an Assistant Research Scientist in the Center for Astrophysics, Space Physics and Engineering Research.

Lorin S. Matthews was born in Paris, TX, in 1972. She received the B.S. and Ph.D. degrees in physics from Baylor University, Waco, TX, in 1994 and 1998, respectively.
She is currently an Assistant Professor with the Physics Department, Baylor University. Previously, she worked with Raytheon Aircraft Integration Systems where she was the Lead Vibroacoustics Engineer on NASA's SOFIA (stratospheric observatory for infrared astronomy) project.

Truell W. Hyde (M'00) was born in Lubbock, TX, in 1956. He received the B.S. degree in physics and mathematics from Southern Nazarene University, Bethany, OK, in 1978 and the Ph.D. degree in theoretical physics from Baylor University, Waco, TX, in 1988.
He is currently with Baylor University where he is the Director of the Center for Astrophysics, Space Physics & Engineering Research (CASPER), a Professor of physics, and the Vice Provost for Research for the University. His research interests include space physics, shock physics and waves, and nonlinear phenomena in complex (dusty) plasmas.